

JGR Atmospheres

RESEARCH ARTICLE

10.1029/2023JD038732

Key Points:

- Faint UV light is first detected at the location of the low-density streamer stem channel during dark periods
- The electronic current in dark periods is in milliamps, much larger than the ionic current or any capacitive displacement current
- There is indeed ionization activity during dark periods in long sparks due to strong reduced electric fields in the residual stem channel

Supporting Information:

Supporting Information may be found in the online version of this article.

Correspondence to:

X. Zhao and M. Becerra,
zhaoxiangen@outlook.com;
marleybec@gmail.com

Citation:

Zhao, X., Becerra, M., Wang, X., Liu, Y., Du, Y., & He, J. (2023). Ionization activity detected during dark periods in long air positive sparks. *Journal of Geophysical Research: Atmospheres*, 128, e2023JD038732. <https://doi.org/10.1029/2023JD038732>

Received 21 OCT 2022

Accepted 24 APR 2023

Author Contributions:

Data curation: Xiangan Zhao

Formal analysis: Yang Liu

Funding acquisition: Yaping Du, Junjia He

Investigation: Xiangan Zhao, Marley Becerra, Xiankang Wang, Yang Liu

Methodology: Xiangan Zhao, Marley Becerra, Xiankang Wang

Resources: Marley Becerra

Supervision: Yaping Du, Junjia He

Writing – original draft: Xiangan Zhao, Marley Becerra

Writing – review & editing: Xiangan Zhao, Marley Becerra

Writing – review & editing: Xiangan Zhao, Marley Becerra

Writing – review & editing: Xiangan Zhao, Marley Becerra

Writing – review & editing: Xiangan Zhao, Marley Becerra

Writing – review & editing: Xiangan Zhao, Marley Becerra

Ionization Activity Detected During Dark Periods in Long Air Positive Sparks

Xiangan Zhao¹ , Marley Becerra² , Xiankang Wang³ , Yang Liu⁴, Yaping Du¹, and Junjia He⁴

¹Department of Building Environment and Energy Engineering, The Hong Kong Polytechnic University, Hong Kong, China, ²School of Electrical Engineering and Computer Science, KTH Royal Institute of Technology, Stockholm, Sweden, ³Electric Power Research Institute, State Grid Hubei Electric Power Co., Ltd., Wuhan, China, ⁴State Key Laboratory of Advanced Electromagnetic Engineering and Technology, Huazhong University of Science and Technology, Wuhan, China

Abstract The dark period in long air gap discharges has been assumed in the literature as the time between consecutive streamer current pulses when ionization and luminosity are absent. These dark periods are also present in natural lightning, in processes such as the inception and propagation of upward positive leaders, the development of needles, as well as transient luminous events in the upper atmosphere. Only recently, faint luminosity has been observed during dark periods, challenging this assumption. This paper aims to study any possible electrical activity during dark periods by means of experiments supported by computer simulation. Therefore, an experimental platform, including low-current measurements, Schlieren and standard photography as well as ultraviolet (UV)-photon detection was used to observe the electrical-optical-thermal characteristics of the dark period. A complementary numerical model was used to estimate the streamer space charge spatial distribution and its drift during dark periods. It is found that faint UV and visible light during the dark period is emitted exactly at the location of the low-density streamer stem channel. This process is accompanied by the generation of an electronic current in the order of hundred microamps to milliamps. The simulation results show that this ionization activity occurs due to strong reduced electric fields in the residual stem channel above 112 Td, which is mainly determined by a combination of applied voltage, space charge distribution, and localized heating. Thus, the presented results show that there is indeed ionization activity during dark periods in long air gaps, which maintains a continuous glow-like discharge.

Plain Language Summary The knowledge of the physical mechanisms of long positive sparks is necessary to solve engineering problems and to understand natural lightning. In these discharge phenomena, dark periods are prevalent, which refers to the time durations without ionization activity between the consecutive and separate streamer bursts. As the name implies, it is traditionally believed that ionization and luminosity are absent during dark periods. Recently, faint visible light was detected in dark periods, challenging the conventional perceptions. To this end, experiments were carried out to observe the electrical-optical-thermal properties of dark periods, and a complementary numerical model was built to estimate the space charge distribution and its drift during dark periods. Results show that in addition to visible light, there is also faint ultraviolet light during dark periods, together with an mA electronic current. Further analysis revealed that there is indeed ionization activity during dark periods in long sparks due to strong reduced electric fields, maintaining a continuous glow-like discharge. These new findings will help to further investigate the inception and stepping processes of positive leaders in both long laboratory sparks and natural lightning, as well as the development of needles and transient luminous events in the upper atmosphere in natural lightning.

1. Introduction

The time duration when no ionization activity is detectable during consecutive, separate positive streamer corona bursts in long air gap experiments is generally referred to as the dark period (Gallimberti, 1979). The dark period is explained by the reduction of the electric field around the highly stressed positive electrode by the space charge left behind after a streamer stops propagating (Les Renardières Group, 1974). This electrostatic shielding effect has been assumed to inhibit the further development of ionization, usually detected in camera images as a dark period without visible illumination. However, if the applied voltage continues increasing, the electric field distribution will also augment until a new streamer is again initiated, ending the dark period. It can take place multiple times both before and after the initiation of a stable positive leader discharge, when it is referred to as the primary or the secondary dark period respectively (Carrara & Thione, 1976). Observe that the dark period that

we make reference to does not take place during any stage of streamer development. Thus, it does not have any relation to the ‘glow at streamer head’ (Ebert et al., 2010; Luque & Ebert, 2010) or the ‘inception cloud’ (Briels et al., 2008; Kochkin et al., 2014a) or to the dark trace behind a propagating streamer head (Liu, 2010; Luque & Ebert, 2014) documented in the literature during streamers development. Furthermore, it is different from the intervals between short streamer discharges under repetitive pulses, without the formation of stems (e.g., Nijdam et al., 2011; Ono & Oda, 2003). Instead, the dark period discussed here takes place after a streamer forming a stem reaches its maximum length (and stops propagating) and before a new streamer is again initiated.

Although the definition of the dark period is derived from long sparks in the laboratory, it is also of great value for the study of several phenomena of natural lightning. First, the primary dark periods are present in the initiation process of upward positive leaders under thunderstorms. As a downward negative leader in natural cloud-to-ground lightning approaches the ground, multiple corona streamer bursts are generated from grounded objects such as towers (e.g., Nag et al., 2021; Visacro et al., 2017). The interval between adjacent corona streamer bursts can be considered a primary dark period. As a result, the initiation of upward positive leaders in long laboratory sparks was also studied by many scholars (e.g., D’Alessandro et al., 2004; Y. Xie et al., 2018). Second, the suspected stepwise progression of upward positive leaders contains a process similar to the secondary dark period. Before each stepping process, the residual discharge channel is decaying without any changes in leader length, until an intense corona streamer burst appears at the leader tip and then a luminosity wave develops toward the ground along the residual channel (Gao et al., 2020; Qie et al., 2019; Visacro et al., 2017). As carriers of ionization waves for the re-illumination process, the evolution of the residual channel in the so-called secondary dark period is crucial for subsequent discharges (Srivastava et al., 2019). Third, the secondary dark period may be also important to study the needles in natural lightning (Hare et al., 2019; Pu & Cummer, 2019; Saba et al., 2020). Saba et al. (2020) observed that needles blinked in slow motion in a sequential mode. During the intervals between these blinks, the intriguing plasma channels also exhibit no obvious ionization activity and luminosity as it happens in dark periods. It is reasonable to speculate, however, that the evolution of the channel during similar dark periods had a non-negligible effect on its subsequent blinks. In addition, the dark period may also link to recoil-type streamers or leaders (B. Wu et al., 2022), which retrace the residual channels created by needles. Furthermore, according to limited observations, dark-period-like processes are possibly present in the transient luminous events in the upper atmosphere (van der Velde et al., 2019).

Due to the intrinsic experimental limitations (e.g., sensitivity) when observing dark periods occurring during natural lightning, research on this subject has focused on dark periods taking place in the laboratory. Observe that only until recently, the electric fields, corona discharge currents, and streamer morphology under outdoor thunderstorms were observed by Arcaño et al. (2021). It was found that the frequency of corona streamer bursts (i.e., the duration of dark periods) is correlated with the ambient electric field for the first time.

However, extensive laboratory experiments have been conducted to measure the duration and frequency of dark periods, including the factors affecting them (Huang et al., 2020; Les Renardières Group, 1974, 1977; Shah et al., 2018; S. Xie et al., 2013). Furthermore, measurements of the charge and the electric field at the positive electrode during dark periods have also been reported (Les Renardières Group, 1974). Thus, it is known that the characteristics of primary dark periods depend on the applied voltage (U), its variation rate (dU/dt) as well as the spatial electric field distribution near the positive electrode (Domens et al., 1991). In turn, the characteristics of secondary dark periods depend mainly on dU/dt and humidity (Chen et al., 2016; Gallimberti, 1979).

In contrast to standard measurements, detailed, high-sensitivity photographic observations during dark periods were reported only until recently. The variation in air density in front of the positive electrode during long primary dark periods has been first observed using high-speed Schlieren photography (Zhao et al., 2017). It has been found that the low-density stem channel(s) formed by the current of filaments converging into the streamer root, develop during the dark period as a growing mushroom expanding with a speed of several m/s. Then, the stem channels expand radially with an average velocity of $5 \mu\text{m}/\mu\text{s}$ as estimated from Schlieren images (Xiao et al., 2019). Later, the radial air temperature in stem channels during the primary dark period has also been estimated with a quantitative Schlieren technique (Cheng et al., 2020). It was found that the measured temperature of the channel during the dark period remained roughly constant or decreased at a low rate. Next, direct optical measurements of faint luminosity at the streamer stem from the second primary dark period were presented by (Zhao, Becerra, et al., 2021). It was shown that the length of the faint bright channel is nearly equal to that of the remaining low-density channel observed in Schlieren images. Furthermore, small current components ($\sim\text{mA}$)

were detected during dark periods. Interestingly, evidence of such small currents has been already reported in early experiments when the measured charge injected in the gap increased slightly during the dark period (Les Renardières Group, 1974). This observation was first interpreted based on two possible causes: the drift of the remaining streamer space charge into the gap or a continuous weak ionization during the dark period (Les Renardières Group, 1974). Following a very simplified theoretical analysis, the drift of the remaining streamer space charge into the gap was attributed as the most reasonable cause for any current or charge excess during dark periods (Les Renardières Group, 1974). This assumption has not been challenged until recently (Zhao, Becerra, et al., 2021; Zhao, Liu, et al., 2021; Zhao, Wang, et al., 2021), in connection to the faint light emission measured during dark periods (Zhao, Becerra, et al., 2021; Zhao, Liu, et al., 2021; Zhao, Wang, et al., 2021). This illumination was attributed instead to an unknown ionization process in the stem taking place under a rising electric field. This ionization could be interpreted as the result of a capacitive current that maintains a sufficiently high electric field in the stem channel (Bazelyan & Popov, 2020).

The duration of dark periods has been predicted by several numerical models for long air sparks (e.g., Gallimberti et al., 2002; Goelian et al., 1997; Y. Xie et al., 2014) and natural lightning (e.g., Becerra & Cooray, 2006a, 2006b) under several simplifying assumptions. First, simple approximations of the streamer space charge spatial distributions are generally assumed. Second, the drift of this streamer space charge into the gap under the existing electric field as well as the presence of the low-density stem channel(s) produced at the streamer root are also neglected. On the other hand, only a few simulations have been reported for the duration of secondary dark periods (Becerra & Cooray, 2008; Y. Xie et al., 2018). They also generally assume that the streamer space charge remains immobile.

Several numerical models evaluating the physical properties of the stems during the dark period have also been published. In all of them, no ionization is assumed to take place during the dark period. In early studies, zero-dimensional (0D) thermalization models have been used to simulate the energy transfer in the streamer stem during the primary dark period (e.g., Gallimberti, 1979). It is suggested that the gas temperature during the primary dark period could increase on its own to the critical temperature of 1,500–2000 K to trigger the streamer-leader transition due to the vibrational-translational (V-T) relaxation. This model has been widely used in later numerical studies on the leader inception (Becerra & Cooray, 2006a; Gallimberti et al., 2002; C. Wu et al., 2013). The predictions of 0D models have been later challenged by one-dimensional (1D) numerical models with a detailed chemical scheme (Liu & Becerra, 2017, 2018). Thus, the stem temperature was shown to decrease instead during dark periods, since conduction losses dominate over V-T relaxation in the absence of any electronic current in the dark period (Liu & Becerra, 2017). However, the predicted trend of stem temperature decay during the dark period has been recently shown to be faster than measurements (Cheng et al., 2020). This disagreement between the modeling theory and measurements had been also attributed to additional heating due to the ionic currents caused by the drift of the remaining space charge (Cheng et al., 2020).

Thus, it has been speculated throughout the literature that the drift of the space charge is the cause of small currents measured during dark periods as well as the disagreement between the measurements and estimations of the stem temperature. However, it is also known that the presence of continuous ionization during the dark period could also explain those observations (Les Renardières Group, 1974; Zhao, Becerra, et al., 2021; Zhao, Liu, et al., 2021; Zhao, Wang, et al., 2021). Since no proper quantitative evaluation of the effect of streamer space charge drift or continuous ionization on measured currents during dark periods exists in the literature, this paper will focus on performing that assessment. For this reason, the experimental platform already used in (Zhao, Becerra, et al., 2021; Zhao, Liu, et al., 2021; Zhao, Wang, et al., 2021) has been upgraded to allow the simultaneous measurement of the optical-electrical-thermal characteristics of the residual channels in dark periods. Furthermore, the measurements are analyzed through complementary numerical simulation of the streamer space charge spatial distribution and its drift during dark periods.

2. Methods

2.1. Experimental Setup

Experiments were carried out on the setup shown in Figure 1a. A positive switching impulse (200/5,000 μ s) generated with a Marx generator was applied to a 1.4-m rod-plane air gap. The rod electrode was located on the high-voltage (HV) terminal and its dimensions were presented in Figure 1b. A conical copper electrode was located at the head of the rod electrode in order to increase the probability of producing a single streamer stem

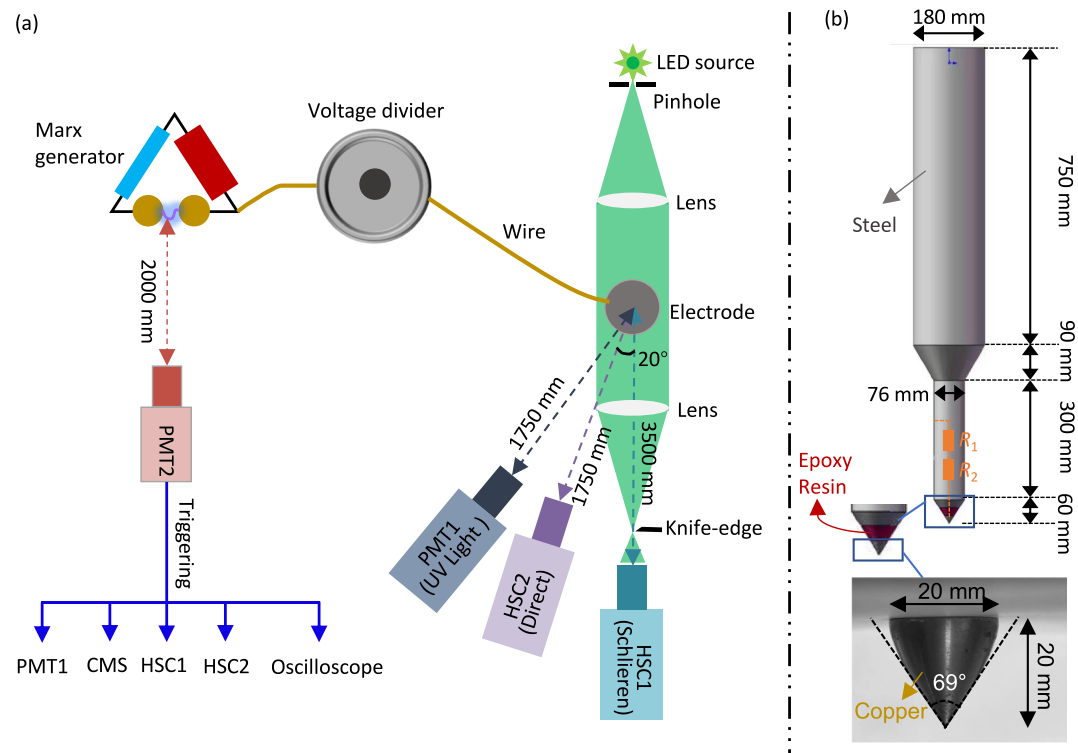


Figure 1. Experimental setups: (a) top view of the experimental arrangement (not to scale) and (b) dimensions of the HV electrode.

at the tip (Yang et al., 2018). The plane electrode was a round aluminum plate with a diameter of 2 m and was well grounded by a copper strip. Peak voltages of 172, 230, 289, and 345 kV were applied for producing multiple streamer bursts with their corresponding dark periods without breakdown. The applied voltage was recorded by a Rigol MSO5104 digital oscilloscope together with a capacitor divider (ratio: 1:586).

The total current in the experiment was measured with two different shunt resistors, that is, R_1 and R_2 in Figure 2a. The epoxy resin was used to electrically isolate the copper electrode tip from the electrode. The resistor R_1 consisted of four 1-k Ω low-inductive resistors in parallel, with an equivalent DC resistance of 250 Ω . The resistor R_2 consisted of eight 100- Ω low-inductive resistors in parallel, with an equivalent DC resistance of 12.5 Ω . The shunt resistors were assembled with a double squirrel cage structure, and its three-dimensional (3D) assembly diagram was shown in Figure 2b. The resistors R_1 and R_2 were connected in series to measure the truncated, small current component (iS) during dark periods, while the resistor R_2 was used alone to measure the complete current of streamer and leader discharges (or the large current component, iL). Figure S1 in Supporting Information S1 shows how the shunt resistors are mounted inside the electrode. The frequency response characteristic of the shunt resistors was measured with a vector network analyzer and plotted in Figure 2c. The total impedance of R_1 and R_2 series connection was almost unchanged up to 10 MHz, while the impedance of R_2 alone remained fairly constant up to 15 MHz. The bandwidth of R_2 can be sufficient to resolve the rise time of the current pulses of first streamer bursts, which is about 10 ~ 50 ns (Gallimberti, 1979; Zhao, Becerra, et al., 2021; Zhao, Liu, et al., 2021; Zhao, Wang, et al., 2021). This resistor will perform even better to resolve the current rise time of subsequent streamers since it is generally longer (Zhao, Becerra, et al., 2021; Zhao, Liu, et al., 2021; Zhao, Wang, et al., 2021). On the other hand, the bandwidth of the series connection $R_1 + R_2$ is well above the requirements to measure the expected DC component flowing during the dark period (Zhao, Becerra, et al., 2021; Zhao, Liu, et al., 2021; Zhao, Wang, et al., 2021). The remaining modules, such as data acquisition (DAQ), electro-optical (E/O) conversion and transmission in Figure 2a, were the same as the current measurement system in (Jiang et al., 2018; Xiao et al., 2019). A gas discharge tube (GDT) was used to protect the data acquisition module.

The low-density stem channels were visualized with a Toepler's lens-type Schlieren imaging system (He et al., 2022). The light path of the Schlieren system was shown in the green area in Figure 1a. For both lenses,

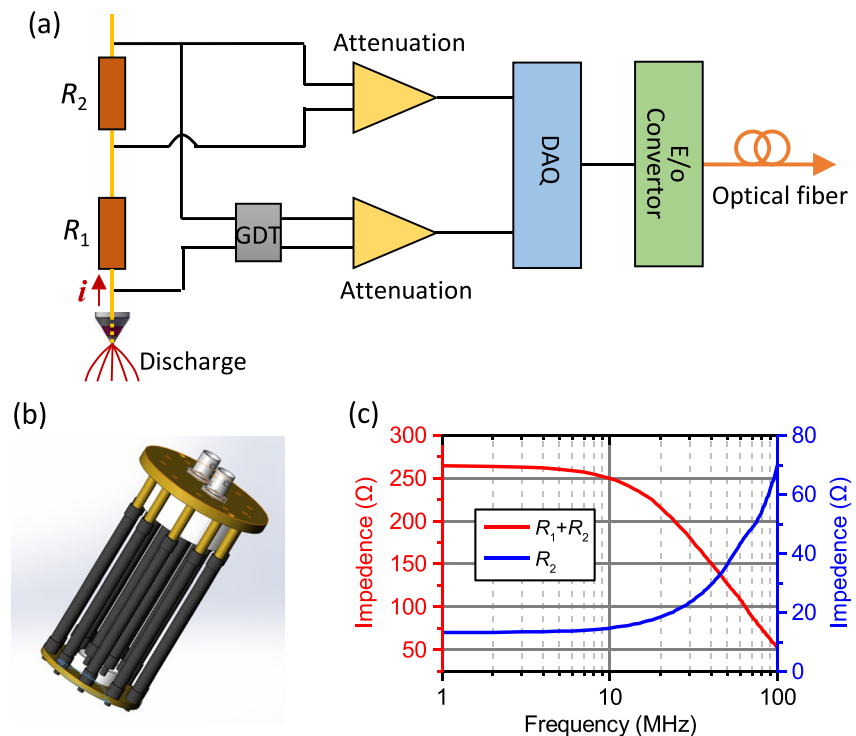


Figure 2. Current measurement system (CMS): (a) the schematic diagram of the measurement system; (b) the 3D assembly diagram of shunt resistors; (c) the frequency response characteristic of the shunt resistors.

the focal length was 1,800 mm and the aperture 150 mm. A pinhole with a diameter of 2 mm and a knife-edge parallel to the air gap axis were located at the focal points of the lenses. A 60-W light-emitting diode (LED) with a central wavelength of 512 nm was applied to illuminate the system. The Schlieren images were recorded with a Photron SA-X2 high-speed camera (HSC1) together with a Sigma 150 ~ 600 mm F/5.6 zoom lens. The camera was operated at 192,307 frames-per-second (fps) with an exposure time of 3.56 μ s. A frame size of 160 \times 256 pixels was used with a corresponding spatial resolution of 200 μ m. The calibration curve of the Schlieren system required to estimate the air density of the stem channel from the photographs (Zhao et al., 2019) is included in Figure S2 in Supporting Information S1.

The streamer morphology was observed with a Phantom V1212 high-speed camera (HSC2) and a Nikon 50 mm F1.4 fixed lens. Camera HSC2 was placed 1.8 m away from the electrode, and the angle between the shooting directions of camera HSC2 and camera HSC1 was about 20°. A digital delay pulse generator (Sapphire 9,200+) was employed to fully synchronize the exposure sequences of the cameras HSC1 and HSC2. Therefore, the camera HSC2 was also operated at 192,307 fps with an exposure time of 3.56 μ s. The corresponding spatial resolution was 128 \times 256 pixels with an observation area of 128 \times 256 mm². According to the spectral response of the camera HSC2 and the transmission of the Nikon lens Figure S3 in Supporting Information S1, the standard photography in this paper was most sensitive to a visible light wavelength between 400 and 800 nm.

In the experiment, long-wave ultraviolet (UV) optical emission (337 nm) was observed by a multianode photomultiplier tube assembly (Hamamatsu, H10515B-103) with a narrow-band-pass filter (in the range between 330 and 340 nm). Note that the UV band-pass filter was used to only detect light emission caused by high-energy electrons produced by glow or streamer discharges. This also will discard any possible low-energy optical emission associated with the decay of vibrational energy as observed in afterglows (Ono, 2018). This photomultiplier system PMT1 in Figure 1a, had 16 channels arranged vertically to measure the UV emission of different sections of the discharge channel. The light cross-talk ratio between different channels was less than 4%. The PMT1 assembly operated in a gain of 2×10^5 under a supply voltage of 600 V. The output signals were recorded with oscilloscope modules (TiePie HS6 DIFF) with a sampling rate of 200 MS/s. In order to calibrate PMT1, the incident light beam was split by a beam splitter after passing through the UV lens set, with one beam projected into the PMT assembly and the other entering the viewfinder with a digital camera. The incident light reached

the PMT assembly and the viewfinder window with the same light range, achieving a 1:1 magnification. With this optical path, the PMT assembly and the camera at the viewfinder had the same viewing area. By dividing the camera's field of view into 16 equal parts, the axial observation range of each PMT channel was obtained, that is, the spatial resolution of PMT1. In these experiments, the electrode tip was located approximately in the center of the first PMT channel and the spatial resolution of PMT1 was estimated to be 5.5 mm. Observe that even though PMT measurements have been utilized already to measure optical emission from streamers and leaders (Dwyer et al., 2008; Kochkin et al., 2012, 2014b; Rahman et al., 2008), they are here used for the first time to detect light during dark periods in long sparks.

In this paper, experiments were divided into two stages. The first stage focused on the current in dark periods, as well as the channel luminosity and gas density variation; while the second stage aimed to measure the UV emission during dark periods. All experiments were conducted on the platform shown in Figure 1, but the PMT1 was not included in the first stage and the Schlieren system was not included in the second one. In the first stage, the testing conditions were temperature of 303 K, absolute humidity of 16.7 g/m³ and atmospheric pressure; while in the second stage, 291 K, 9.2 g/m³ and atmospheric pressure. In the experiments, all devices were triggered by the output signal of a single anode PMT module (PMT2) in Figure 1a, which was used to detect the ignition of the first spark gap of the Marx generator.

2.2. Numerical Model

Estimating the current produced by the drift of the streamer space charge during the dark period is key to evaluating its contribution to the total current measured in the experiment. Such a calculation requires two different steps. First, the estimation of the spatial distribution of the charge injected by each streamer burst into the gap. Second, the calculation of the current produced by the drift of this space charge during the dark period.

Although the physical properties of single or few short streamer filaments can be calculated in detail using microscopic particle or fluid models (e.g., Marskar, 2019), they cannot be used up to date to estimate the spatial distribution of an entire streamer burst having multiple ensembles of numerous filaments. On the other hand, simplified macroscopic physical models of branched discharge trees can provide qualitative information of centimetre-long streamer trees (Luque & Ebert, 2014). However, they are still limited to delivering quantitative estimates of macroscopic properties (e.g., charge) as to allow a one-to-one comparison with experimental results. Thus, consistent physical approaches cannot yet be used to estimate the final charge distribution left behind a fully extended, branched streamer bursts (after propagating several tens of centimeters) in long air gaps.

Thus, simplified approaches have been used instead in the literature to describe the spatial charge distribution of long streamers. Early approaches represented the streamer as a point charge source or assume a known charge distribution within a given region (Les Renardières Group, 1974). However, later studies have successfully estimated the total charge of streamer bursts (e.g., Becerra & Cooray, 2006a; Goelian et al., 1997) in agreement with experimental results. These studies assume that the electric field with a streamer burst after it stops propagating, is roughly constant and equal to the stability field E_{str} . Even though physical models have shown that a constant electric field inside the streamer contradicts the conservation of charge (Luque & Ebert, 2014), measurements have shown that the electric field produced by the collective of filaments within the streamer volume is roughly uniform and equal to E_{str} (Petrov et al., 1994). Given the experimental evidence supporting the assumption of a constant E_{str} behind the streamer front and the usefulness of this concept to deliver estimates in agreement with measurements, it is currently the only available tool to calculate the macroscopic properties (such as spatial extension and charge) of long streamers. Even though most of the studies using the concept of the stability field only estimate the total streamer charge, the complete streamer spatial distribution can be fortunately calculated with the method presented in (Becerra, 2014).

Thus, the spatial distribution of the charge density left behind by each fully developed streamer burst is here calculated by solving the inverse source problem for the Poisson equation through optimization (Becerra, 2014). Observe that in contrast to the direct solution of the Poisson equation, the inverse source problem aims to estimate the charge distribution from a known voltage distribution. Since measurements have shown that the electric field within a streamer burst keeps a constant stability field E_{str} (Petrov et al., 1994), the streamer potential distribution ϕ_{str} is defined by the product of E_{str} and the shortest distance between the point (r, z) to the electrode surface. This assumed distribution is then used here to calculate the unknown net streamer charge distribution function

$\rho_{\text{str}}(r, z)$. In the presence of an existing charge density $\rho_0(r, z)$ left behind by previous bursts (with $\rho_0 = 0$ for the first streamer but $\rho_0 \neq 0$ for the subsequent bursts), the calculated potential distribution ϕ within the streamer was defined as:

$$\nabla^2 \phi(r, z) = -\frac{\rho_{\text{str}}(r, z) + \rho_0(r, z)}{\epsilon_0} \quad (1)$$

and then an optimization procedure was used to find the streamer charge distribution $\rho_{\text{str}}(r, z)$ that minimizes the squared error between the calculated potential ϕ and the assumed streamer potential ϕ_{str} . Outside the streamer region, the direct solution of the Poisson equation was calculated as:

$$\nabla^2 \phi(r, z) = -\frac{\rho_0(r, z)}{\epsilon_0} \quad (2)$$

The search for the net charge distribution $\rho_{\text{str}}(r, z)$ at the extinction of each streamer burst was performed using a gradient-based optimization algorithm. Details of the implementation of the optimization problem can be found elsewhere (Becerra, 2014). Observe that the calculated $\rho_{\text{str}}(r, z)$ after the streamer stops propagating has the same polarity as the electrode. Although negative and positive ions are produced during the streamer propagation (Nijdam et al., 2020), the space charge left behind by the extinct streamers in the experiments is known to be dominated by positive ions. This is consistent with laboratory measurements showing a decrease in the surface electric field of positive electrodes after streamer extinction as the result of the space charge electrostatic shielding (Les Renardières Group, 1974). Once the streamer charge distribution in front of the electrode was calculated for each extinct streamer, the total field distribution including the space charge distortion of the Laplacian field can be computed during the dark periods.

The drift of the charge left behind by each extinct streamer burst can be readily calculated during the dark period once the first step is concluded. In the case of the first streamer burst, its space charge distribution $\rho_{\text{str}}(r, z)$ drifts away from the electrode in the absence of any space charge from a previous streamer ($\rho_0(r, z) = 0$). In general, the drift of the positive charge distribution in the gap $\rho(r, z)$ was calculated by using (Zhao et al., 2017):

$$\nabla \cdot E = -\frac{\rho(r, z)}{\epsilon_0} \quad (3)$$

$$\frac{\partial \rho(r, z)}{\partial t} + \nabla \cdot \vec{j} = 0 \quad (4)$$

where E is the electric field in the gap and \vec{j} is current density, given by the sum of three contributions, that is, drift due to electric field, advection, and diffusion:

$$\vec{j} = \rho(r, z) \cdot (\mu_i \nabla \phi(r, z) + \vec{v}) - D_i \nabla \rho(r, z) \quad (5)$$

where μ_i is the ion mobility and D_i is the ion diffusion coefficient with values for positive ions taken from (Liu & Becerra, 2016). In the absence of forced convection in the laboratory and neglecting the gas transport produced by any shockwave (Zhao et al., 2017), the gas velocity \vec{v} was assumed equal to zero. The initial solution for the solution of Equation 4 was $\rho_{\text{(init)}}(r, z) = \rho_{\text{str}}(r, z) + \rho_0(r, z)$. The measured voltage at each streamer initiation time was used as input for the boundary conditions for the solution of Equations 1 and 2 in the first step. The measured voltage during the dark periods was used for the transient calculation of Equation 3 for the space charge drift calculation step.

The calculation of the second streamer space charge distribution was performed at the end of the first dark period drift calculation. For this calculation, the space charge distribution ρ calculated with Equation 4 at the second streamer inception time defined the pre-existing charge ρ_0 . Then, the drift of the total charge in the gap was calculated during the second dark period. A similar two-step procedure was repeated for the calculation of the third streamer and its corresponding dark period. Then, the ionic current I_p produced by the drift of the space charge in the gap can be calculated as (Morrow & Sato, 1999):

$$I_p = \frac{1}{V_a} \int_V \vec{j} \cdot \vec{E}_L dv \quad (6)$$

where $\int_V dv$ is a volume integral over the discharge space, V_a is the applied voltage and \vec{E}_L is the Laplacian electric field.

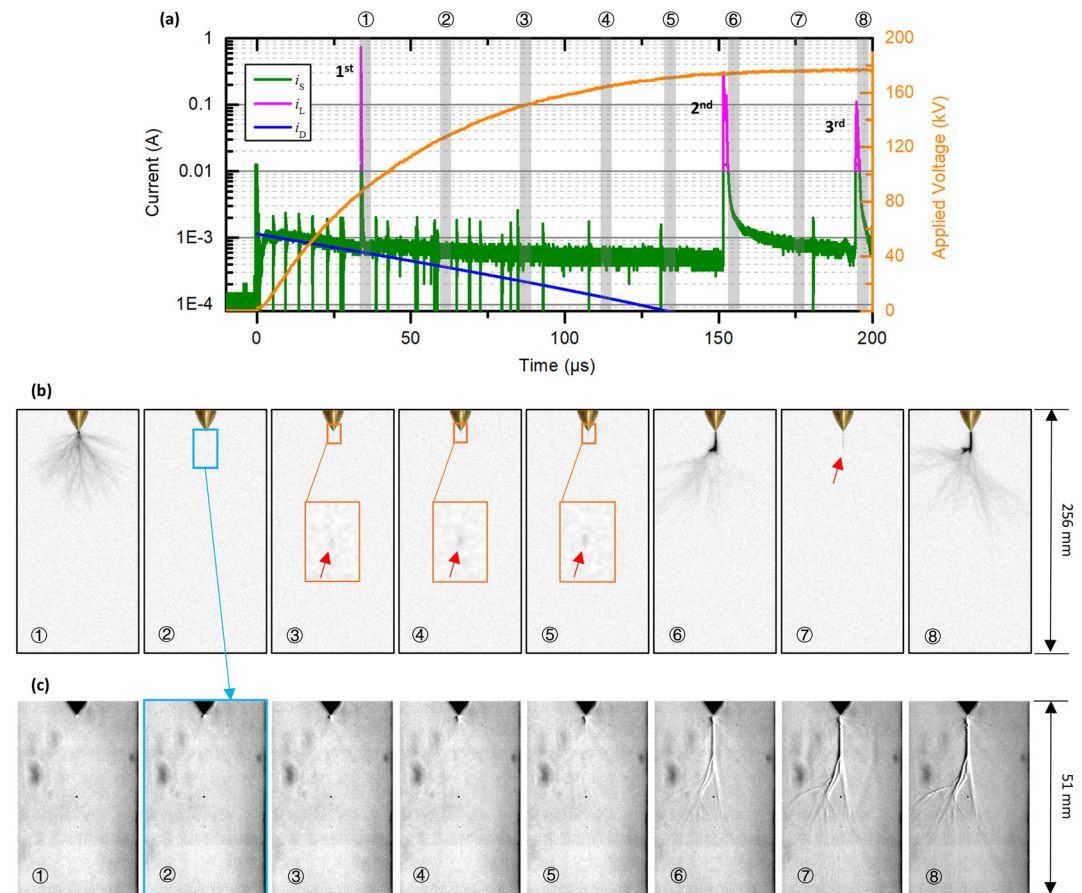


Figure 3. Typical results in the first stage of the experiments. (a) Current and voltage waveforms. Three current components are included, that is, the small discharge current component i_s , the large discharge current i_L , and the displacement current i_D . The dark-period current (i.e., i_s - i_D) is shown in Figure S4 in Supporting Information S1. (b) High-speed standard images of the morphology of streamer bursts and the residual channel, which are color inverted. (c) High-speed Schlieren images of the stem channels, which are contrast enhanced. The observation range for (c) is indicated in (b) by the blue box. The number of each frame in (b) and (c) corresponds to the timing sequence marked with the same number at the top of (a).

3. Results

3.1. Experimental Results

Figure 3 shows typical current and voltage waveforms measured under a switching impulse peaked at 172 kV. The two measured current components are shown in Figure 3a, that is, namely the large current (i_L) and the small current (i_s) components. The calculated displacement current (i_D) flowing through the stray capacitance of the air gap, which is superimposed on the current in the discharge, is also included in Figure 3. This current i_D is estimated by multiplying the first-order derivative of the applied voltage by the gap capacitance (of about 0.32 pF). This gap capacitance was estimated from the measured voltage and current before the first corona streamer burst (see waveforms in Figure 3a at $t = 0 \sim 33.4 \mu\text{s}$) using the method proposed by Y. Li et al. (2021). Observe that the large-amplitude component of the discharge current cannot be measured by the shunt resistors R_1 and R_2 since it is truncated by the GDT at about 0.01 A. Similarly, the small-amplitude component of the discharge current cannot be measured by the shunt resistor R_2 due to its lower sensitivity. As a result, the total current can be obtained by superimposing the large and small current components. Note that the pulse in i_s at $t = 0 \mu\text{s}$ as well as the oscillating signals superimposed to the continuous component are noise produced by electromagnetic interference from the ignitions and burning for the arcs in the spark gaps of the Marx generator.

As can be seen, the current measured during the dark periods does not correspond to a displacement current i_D . Although the current measured before the first streamer burst ($t < 33.4 \mu\text{s}$) obviously corresponds to i_D , the i_s measured afterward cannot be explained by a capacitive current in response to the time variation of the applied

voltage. After the first streamer burst initiates with a peak current pulse of 0.77 A, i_D gradually decreases reaching less than 0.1 mA at $t = 125 \mu\text{s}$. This value is well below the measured current ($i_S = 0.53 \text{ mA}$) at the same time, which was more than five times larger than i_D . The first dark period ends when the second streamer develops producing a current pulse with a peak amplitude of 0.30 A at $t = 151.4 \mu\text{s}$. Subsequently, the discharge enters the second dark period, during which i_S gradually decreases from about 1.0 to 0.7 mA. During this period, i_S is more than one order of magnitude larger than i_D . The second dark period ends at $t = 194.6 \mu\text{s}$ by the initiation of the third streamer burst, having a current pulse peaked 0.12 A.

Standard photographs of the morphology of the first three streamer bursts and the faint luminosity detected during dark periods are shown in Figure 3b. Observe that the morphology of the streamer filaments, as well as the elongation of the streamer stem, is as widely reported in the literature (Gu et al., 2020; Kostinskiy et al., 2018; Zhao, Becerra, et al., 2021; Zhao, Liu, et al., 2021; Zhao, Wang, et al., 2021; Zeng & Chen, 2013). However, it can be seen from the enlarged images that a faint channel is first detected in front of the electrode tip during the first dark period after $t = 69.2 \mu\text{s}$, as marked by the red arrow. The length of the faint channel ranges from 1 to 3 mm. During the second dark period, a longer thin luminous track having a length of 19 mm keeps on emitting light at the location of the main streamer root area. In our previous work (Zhao, Becerra, et al., 2021; Zhao, Liu, et al., 2021; Zhao, Wang, et al., 2021), no bright light channel was detected during the first dark period while it was visible only during the subsequent dark periods. According to the spectral response of the standard imaging system in Figure S3 in Supporting Information S1, the faint luminosity observed in Figure 3b is emitted within the wavelength range between 400 and 800 nm. Furthermore, observe that the second streamer burst after the first primary dark period (see image © in Figure 3b) forms from the head of the stem produced by the first streamer burst. This is different compared with the case when no stem is formed, in which the second streamer would originate from the electrode surface as in the simulations by Niknezhad et al. (2021).

The Schlieren images in Figure 3c provide a closer look at the region where the faint luminosity was detected. They show the variation in air density due to heating caused by streamer currents converging into stems. As can be seen, a small stem with low density having a length of about 0.6 mm is formed at the electrode tip during the first streamer burst. In this stem, the filaments of the first streamer converge as shown in Figure 3b. The streamer stem grows continuously during the dark period reaching about 3 mm before the start of the second corona burst. After the second streamer burst, the low-density stem elongates further and branches as already reported by (Zhao, Becerra, et al., 2021; Zhao, Liu, et al., 2021; Zhao, Wang, et al., 2021). The main channel does not show significant elongation during the second dark period and remains at about 18 mm. After the third streamer burst, the stem branch to the left of the main channel is heated and several small branches appeared. Interestingly, the main stem has the same length and location as the region of faint luminosity observed during the dark periods in Figure 3b. This result confirms that the luminosity here detected in the standard photographs during the dark period is emitted by the low-density stem region.

The measurements with the photomultiplier system PMT1 also showed that the faint luminosity detected by the standard photographs during the dark period has also a significant UV component. Figure 4 shows the experimental results obtained at a higher voltage (250 kV), necessary to measure with a reasonable signal-to-noise ratio in PMT1. In this event, the current components have similar features as those already discussed in Figure 3a, but with larger values during the dark period. The colored bands in Figure 4b illustrate the observation line of sight of each PMT channel in relation to the position of the discharge channel in the standard images. Figure 4c presents the corresponding time-resolved UV emission signals of the different sections of the discharge channel. As expected, all three streamer bursts produce pulsed UV irradiance (Arcanjo et al., 2021). However, the UV emission detected during the dark periods was about two orders of magnitude smaller than that measured during the preceding streamer burst. For that reason, the UV emission during the first dark period was well below the detection level of PMT1. Fortunately, significant UV signals were observed for channels CH1–CH3 after the intense emission of the second streamer burst. The detected UV emission from these three channels covers the exact observation region where the stem channels look the brightest in the photographs. Further, it can be found that the UV emission is most intense closest to the electrode.

3.2. Simulation Results

Numerical simulation results of the event shown in Figure 3 were here used to give further input for the interpretation of the measurements during the dark period. Figure 5 shows the charge density and electric field distribution estimated after the development of the first streamer burst and during the first dark period. The estimated charge

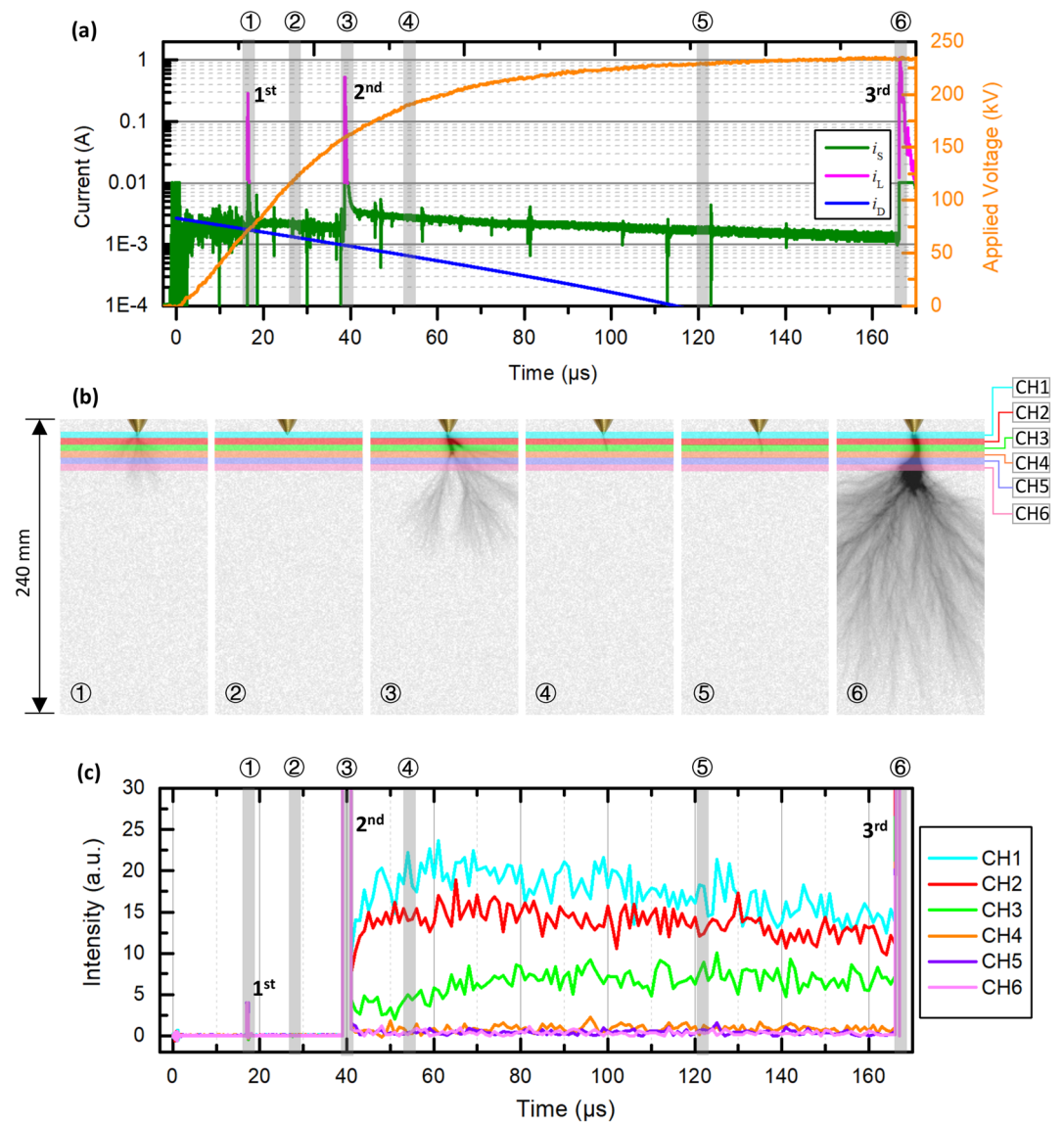


Figure 4. Typical observations in the second stage of the experiments. (a) Current and voltage waveforms. The dark-period current (i.e., i_s - i_D) is plotted in Figure S5 in Supporting Information S1. (b) High-speed standard images with color inverted. (c) Time-resolved UV irradiance (330–340 nm). The observation area covered by each channel corresponds to the same color bar in (b).

distribution of the first streamer charge follows a bathtub distribution, having a maximum density of 0.2 C/m^3 in the close proximity of the electrode that gradually falls to $5 \times 10^{-4} \text{ C/m}^3$ before increasing again at the streamer front. This charge is distributed within a volume (in Figure 5a) well within the streamer region as observed in Figure 3b ①. With this charge distribution, the average electric field within the streamer zone at inception is rather constant and equal to the assumed stability field E_{str} . The total charge of this first streamer burst is calculated as $2.4 \times 10^{-8} \text{ C}$ corresponding to an apparent charge of $1.8 \times 10^{-8} \text{ C}$. This last estimated value is in good agreement with the apparent charge of $1.6 \times 10^{-8} \text{ C}$ obtained by integrating the measured first streamer current peak in Figure 3a. Under the influence of the increasing applied voltage during the first dark period, the space charge drift leads to the fast recovery of the electric field in front of the electrode $E_{\text{tip}} = E(r=0, z=0)$. Observe in Figure 5e that E_{tip} at $t = 50 \mu\text{s}$ already reached values above the ionization threshold ($E_{\text{crit}} \sim 3 \times 10^6 \text{ V/m}$) at atmospheric density as the result of the charge density drop in front of the electrode by the 2 mm drift of the space charge. Assuming that no further ionization is produced during the dark period, the electric field distribution in front of the electrode estimated at $t = 100 \mu\text{s}$ even exceeds the original Laplacian electric field at the first streamer

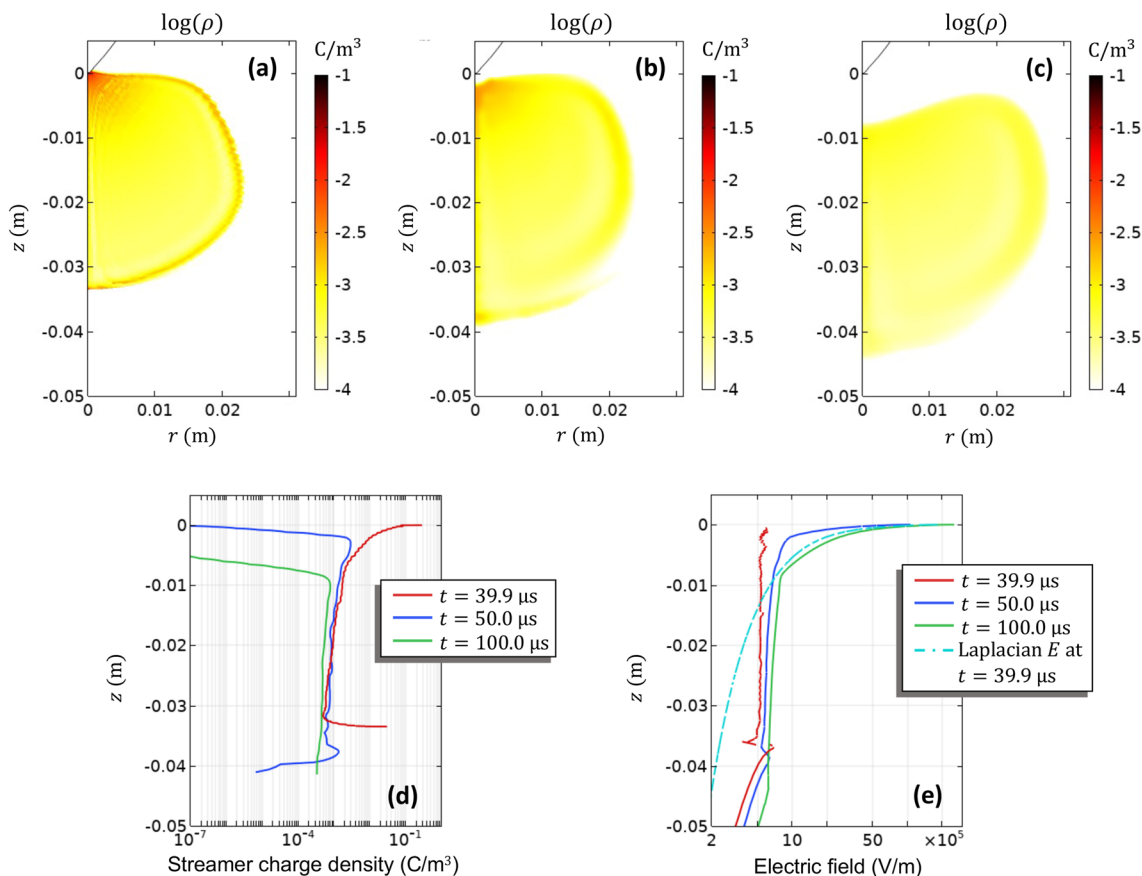


Figure 5. Calculated charge distributions (a) after the first streamer development at $t = 39.9 \mu\text{s}$ and during the dark period at (b) $t = 50 \mu\text{s}$ and (c) $t = 100 \mu\text{s}$. The charge density distribution and electric field distribution in front of the electrode along the symmetry axis are shown in (d and e), respectively. The Laplacian electric field at the first streamer inception time is also included in (e).

inception time. This result shows that the electrostatic conditions in front of the electrode become favorable to start ionization in the gap already during the dark period, much earlier than the time when the second streamer is initiated (at $t = 151.7 \mu\text{s}$).

Figure 6a shows the total charge density estimated soon after the development of the second streamer. In this case, the convergence point of the filaments in the second streamer zone is taken at a distance of 2 cm from the electrode as observed in the photograph in Figure 3b. The total charge of the second streamer is estimated as $1.1 \times 10^{-7} \text{ C}$ in the presence of the pre-existing drifted charge of the first streamer. Since most of the second streamer charge is injected in a region a few centimeters ahead of the electrode tip, the left space charge cloud drifts in a region with a relatively low electric field. Since the applied voltage after the second streamer does not increase significantly, the space charge drifts and diffuses during the second dark period only a few millimeters as shown in Figure 6b.

The simulation results also allowed quantifying the total ionic current produced by the drift of the space charge injected by the first and second streamers during the dark periods. As can be seen in Figure 6c, the drift of the first streamer produced an ionic current reaching a maximum of $12 \mu\text{A}$ while the drift of the total charge during the second dark period reached a peak below $22 \mu\text{A}$. These ionic currents are more than one order of magnitude smaller than the measured currents (in the order of several hundred μA in Figure 3a) during dark periods. Thus, these simulation results show that the significant currents here measured during the dark periods cannot be attributed neither to ionic currents due to space charge drift nor to a displacement current.

4. Continuous Weak Ionization Produced During Dark Periods

The results described in the previous section show that the current and light emission here measured cannot be attributed to the ionic currents produced by the drift of the streamers' space charge, contrary to what has been

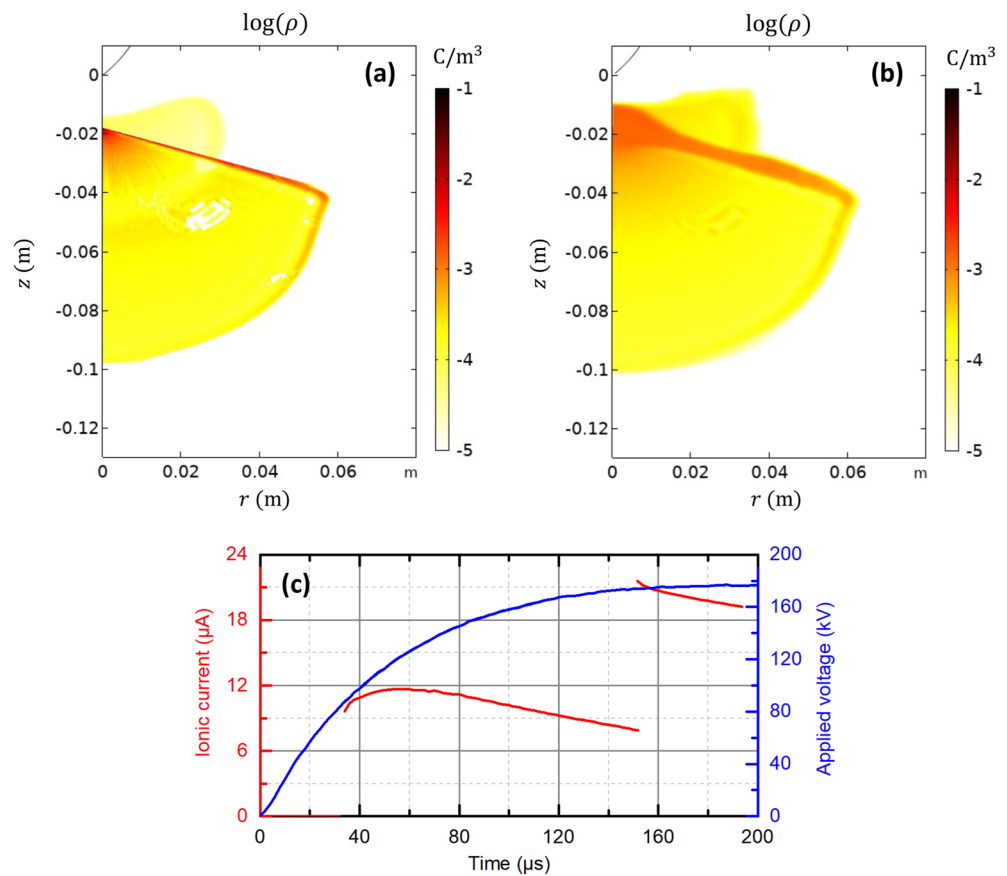


Figure 6. Charge distributions calculated (a) after the second streamer development at $t = 151.7 \mu s$ and (b) estimated ionic current due to the space charge drift with the applied voltage included as reference.

previously assumed in the literature (Les Renardières Group, 1974). Similarly, they cannot be interpreted to be caused by displacement currents that maintain a sufficiently high electric field in the stem channel (Bazelyan & Popov, 2020). Even though it has been shown that a voltage derivative $dU/dt > 1 \text{ kV}/\mu s$ can produce a capacitive current that maintains a sufficiently high electric field in the stem channel of $E/N = 70\text{--}90 \text{ Td}$ (Bazelyan & Popov, 2020), the currents during the dark period were also here detected under an applied voltage weakly changing in time with dU/dt lower than $0.7 \text{ kV}/\mu s$. Therefore, it is pertinent to further analyze the hypothesis that our measurements during the dark period were caused by continuous weak ionization by other conditions.

Although ionization in gases depends on the existing electric field E , it also depends inversely on the particle density N of the medium (Gallimberti, 1979). On one hand, the electrostatic simulation results discussed in the previous section have shown that the electric fields in front of the electrode can reach values larger than the critical threshold required for ionization at atmospheric density. On the other hand, the Schlieren images above and reported in other previous publications (e.g., Zhao et al., 2017; Zhao, Becerra, et al., 2021; Zhao, Liu, et al., 2021; Zhao, Wang, et al., 2021) have also shown that the gas density in front of the electrode is lower than atmospheric due to the presence of the stem. Therefore, it is better to assess the presence of ionization during the dark period instead as a function of the ratio E/N , known as the reduced electric field. The critical $(E/N)_{\text{crit}}$ at which the rate of ionization is larger than attachment in humid air is about 112 Td under the conditions of the test here described in (B. Li et al., 2018).

Since both the electric field and the density in front of the electrode change in space, it is necessary to know their spatial distribution in order to assess where continuous ionization activity could actually take place. For this reason, the spatial distribution of the electric field in front of the electrode for the event in Figure 3 is calculated at the start of the second dark period ($t = 154 \mu s$) under the injected streamer space charge. Although the maximum calculated fields in front of the electrode reach values up to about $3 \times 10^7 \text{ V/m}$, the results in Figure 7 are shown

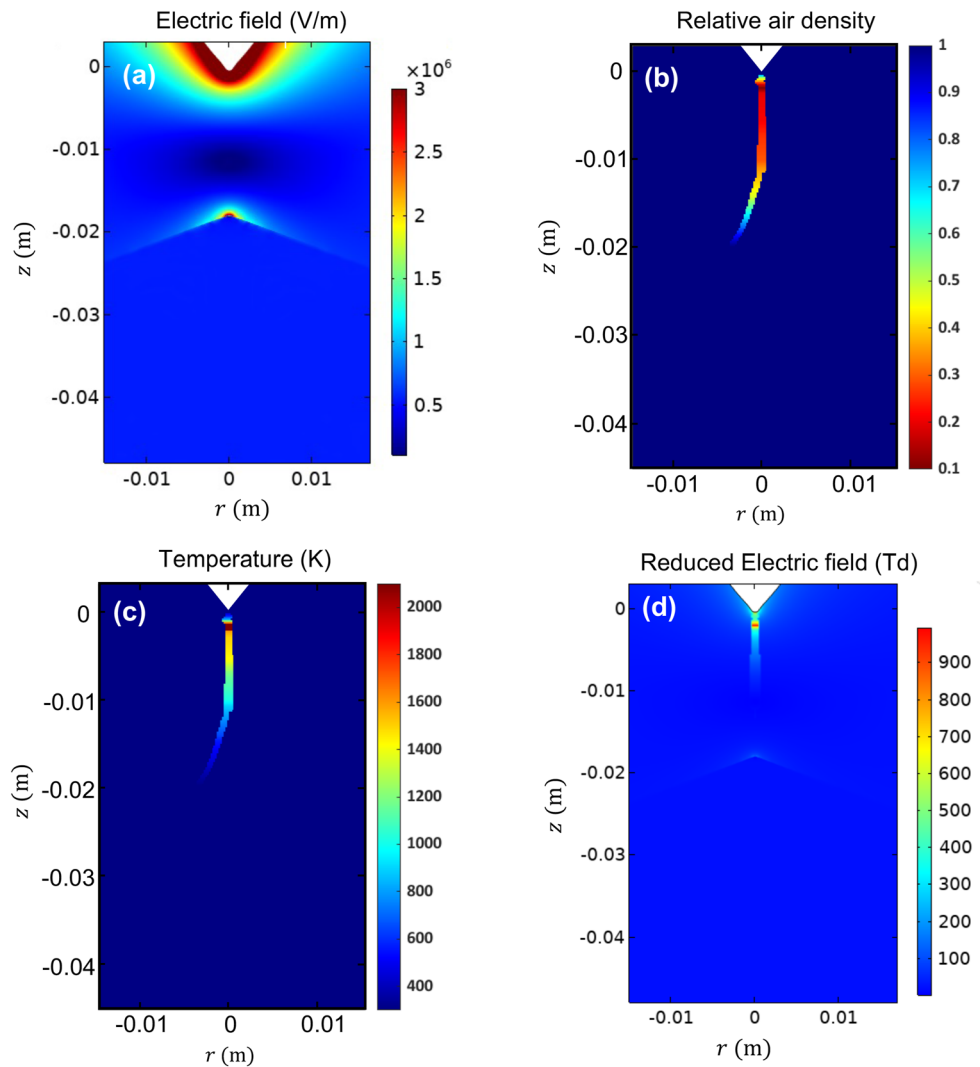


Figure 7. Spatial distribution of (a) electric field, (b) relative density, (c) temperature and (d) reduced field at the start of the second dark period in the event shown in Figure 3.

with the upper limit of the color legend truncated at the ionization threshold E at atmospheric density (for better visualization). The corresponding air density estimated by the method presented by (Zhao et al., 2019; Zhao, Becerra, et al., 2021; Zhao, Liu, et al., 2021; Zhao, Wang, et al., 2021) from the Schlieren image ⑦ in Figure 3c, is also shown in Figure 7b. This low density is caused by the localized heating of the stem as shown in the temperature plot in Figure 7c. Interestingly, the reduced electric field E/N distribution calculated in Figure 7d clearly shows that ionization at the start of the dark period is most intense within the section of the stem closest to the electrode. In this case, the reduced field is significantly larger than $(E/N)_{\text{crit}}$, starting at 650 Td in front of the electrode and then reaching more than 900 Td (in this case) some millimeters in front of the electrode surface. Then, the reduced field decreases as the distance to the electrode increases, reaching $(E/N)_{\text{crit}}$ at a distance of 6 mm. Thus, Figure 7d explains why the faint luminosity observed in the second dark period in the standard photograph ⑦ in Figure 3b corresponds exactly to the narrow area where the stem was formed. Since the stem section where the initial reduced field is larger than $(E/N)_{\text{crit}}$ has a length of only 6 mm, an ionization wave must have further propagated within the low-density stem channel until it reaches the maximum length of 20 mm observed in the corresponding photograph.

The results in Figure 7 show solid evidence that ionization within the dark period can be produced due to the strong reduced electric field in the residual stem channel, as the result of the Laplacian electric field distribution, the space charge distribution and the localized heating of the streamer root. This ionization will allow the

formation of a glow-like discharge within the stem during the dark period, granted that free initial electrons are continuously produced at the location where the reduced electric field is equal to $(E/N)_{\text{crit}}$. Köhn et al. (2018) also found in their experiments that the perturbed air in relation to shock waves or heating could lead to local regions of enhanced ionization. Photoionization is likely to be the main mechanism driving the supply of free electrons. On one hand, the reduced electric fields present within the stem at the start of the dark period are sufficiently high for the excitation of high energy levels as is evident from the UV photons here detected in Figure 4. Observe that UV photons not be produced during the dark period in the absence of ionization as in the case of afterglows (after switching off an active discharge) (Ono, 2018).

Using the current measured during the second dark period and the diameter of the stem channel from the Schlieren images in Figure 3, the current density within that glow-like region is estimated between about 400 and 1700 A/m². Interestingly, the steady-state reduced electric field in glow discharges measured in air under high temperatures and within the same current density range and similar diameters are reported between 35 and 45 Td (Cejas et al., 2020). The corresponding electron density necessary to maintain those currents ranges between 10¹⁷ and 10¹⁸ m⁻³.

The presence of ionization and the formation of a glow-like discharge during the dark period has several unaccounted implications when evaluating the breakdown in long air gaps. Since the existing thermo-hydrodynamic numerical models during the dark periods neglect the electron density during dark periods (Cheng et al., 2020; Liu & Becerra, 2017, 2018), it is then unsurprising that simulations have predicted a faster decay of the stem temperature compared to measurements (Cheng et al., 2020). Since the current density during the glow-like discharge is much lower than that produced for streamers and since electronic fast heating is also low at 35–45 Td (Liu & Becerra, 2017), no increase in the stem temperature should be possible during the dark period. Instead, most of the energy injected by the glow-like discharge would be transferred to vibrational excitation, the dominating process during the dark period. This process will compensate for the drop in the vibrational molecule density as the result of the vibrational-to-vibrational VV relaxation, limiting the drop in temperature in the stem channel during the dark period. Furthermore, the glow-like discharge will inject space charge in the gap (as each of the streamer bursts), but this charge will accumulate only along the narrow stem channel. This highly localized space charge density will further distort the electric field distribution in front of the electrode. This will in turn make the evaluation of the initiation of subsequent streamer bursts after each dark period more difficult to perform.

Consequently, numerical models evaluating the duration and thermodynamic properties of dark periods in long air gaps need to be improved. On one hand, observe that the existing models used to predict the duration of dark periods generally assume that the only space charge in the gap is generated by the streamer bursts and that it also remains immobile (Becerra & Cooray, 2006b; Gallimberti et al., 2002; Goelian et al., 1997; Y. Xie et al., 2014). However, this assumption is not correct in the presence of a glow-like discharge strongly distorting the background electric field distribution. On the other hand, the thermodynamic numerical models assessing the temperature conditions at which the streamer-to-leader transition takes place after dark periods (Liu & Becerra, 2017, 2018) also need to be improved by including the non-zero electronic current between streamer bursts. This current would flow along a “glowing” narrow stem channel with a significantly distorted electric field distribution along the axial direction. In such a case, the channel electric field cannot be calculated assuming a linear recovery during the dark period (Liu & Becerra, 2017, 2018) or even roughly estimated by using Ohm’s law. Instead, it would require at least the two-dimensional calculation of the electric field, which will also lead to changes in the chemistry of the discharge along the axial direction (in addition to the radial changes already included in the recent models).

The above-described effects of a continuous glow-like ionization between streamer bursts also highlight our opinion that the widely used technical term “dark period” in long air gaps can be misleading and inappropriate. Although this continuous ionization has not been detected or understood in the literature before, using the term “dark period” in the future will continue downplaying the presence of additional ionization physical processes that are taking place and affect the sequence of events leading to a breakdown. For that reason, it is here proposed to refer to the time between positive streamer bursts in long air gaps as a “weak-ionization period”. Using this new term can bring attention to the scientific community about a series of electronic processes that have been up to now ignored. It will also make scientists and engineers aware of the glow-like discharge between streamer bursts, which should be accounted for when interpreting experimental observations in the laboratory as well as in nature (as in the case of lightning discharges).

In addition, the work in this paper will also inspire studies on dark-period-related phenomena in natural lightning. In the case of the inception of upward positive leaders, the ionization activity during dark periods may have a significant effect due to the more rapidly changing background electric field and the larger residual heated channel size. In order to quantitatively assess this effect, it is necessary to accurately measure the electronic currents during dark periods. Such a measurement is currently difficult to achieve due to the low signal-to-noise ratio of current measurement devices, which should be further improved. Observe that these discussions above may also apply to the suspected stepping process of upward positive leaders. However, for the needles and transient luminous events in the upper atmosphere, it is impossible to measure the current during dark periods, and it is also difficult to detect the luminosity in dark periods. To investigate the role played by dark periods in these two phenomena, it is possible to extrapolate laboratory data through the main factors affecting the dark period currents, that is, the varying rate of the background electric field, the length of the residual channel, etc. Then numerical models can be applied to simulate the effect of dark period currents on the residual channel.

5. Conclusions

The optical-electrical-thermal characteristics of stem channels in dark periods were simultaneously measured with an upgraded experimental platform. Furthermore, the streamer space charge spatial distribution and its drift during dark periods were built using a complementary numerical model. Based on experimental and simulation results, the ionic and electronic currents in dark periods were estimated, and the mechanism for the electronic current generation was discussed. The main conclusions are as follows.

1. The ionic current due to space charge drift is in the order of μA during the dark period, while the electronic current ranges from hundred microamps to milliamps. The electronic current is not only related to the applied voltage, but also to the charge generated by the previous streamer bursts.
2. The electronic current in the dark period is produced by ionization activity in the stem channel, maintaining a continuous glow-like discharge. This process is induced by the high reduced electric field in the stem due to the electric field distribution, the streamer space charge drift and the thermodynamic processes at the streamer root.
3. The ionization activity at the stem channel closest to the electrode during the dark period is most intense and accompanied by stronger ultraviolet irradiance.

Data Availability Statement

The data can be accessed at the WDC for Geophysics, Beijing (<https://doi.org/10.12197/2023GA007>).

References

- Arcanjo, M., Montanyà, J., Urbani, M., & Lorenzo, V. (2021). Optical signatures associated with streamers and leaders of laboratory discharges. *Geophysical Research Letters*, *48*(20), e2021GL095601. <https://doi.org/10.1029/2021gl095601>
- Bazelyan, E. M., & Popov, N. A. (2020). Stepwise development of a positive long spark in the air. *Plasma Physics Reports*, *46*(3), 293–305. <https://doi.org/10.1134/s1063780x20030022>
- Becerra, M. (2014). On the estimation of the charge of positive streamers propagating in air. *IEEE Transactions on Dielectrics and Electrical Insulation*, *21*(2), 627–634. <https://doi.org/10.1109/tdei.2013.004272>
- Becerra, M., & Cooray, V. (2006a). A self-consistent upward leader propagation model. *Journal of Physics D: Applied Physics*, *39*(16), 3708–3715. <https://doi.org/10.1088/0022-3727/39/16/028>
- Becerra, M., & Cooray, V. (2006b). Time dependent evaluation of the lightning upward connecting leader inception. *Journal of Physics D: Applied Physics*, *39*(21), 4695–4702. <https://doi.org/10.1088/0022-3727/39/21/029>
- Becerra, M., & Cooray, V. (2008). Laboratory experiments cannot be utilized to justify the action of early streamer emission terminals. *Journal of Physics D: Applied Physics*, *41*(8), 085204. <https://doi.org/10.1088/0022-3727/41/8/085204>
- Briels, T., Van Veldhuizen, E., & Ebert, U. (2008). Positive streamers in air and nitrogen of varying density: Experiments on similarity laws. *Journal of Physics D: Applied Physics*, *41*(23), 234008. <https://doi.org/10.1088/0022-3727/41/23/234008>
- Carrara, G., & Thione, L. (1976). Switching surge strength of large air gaps: A physical approach. *IEEE Transactions on Power Apparatus and Systems*, *95*(2), 512–524. <https://doi.org/10.1109/t-pas.1976.32131>
- Cejas, E., Mancinelli, B., & Prevosto, L. (2020). Modelling of an atmospheric-pressure air glow discharge operating in high-gas temperature regimes: The role of the associative ionization reactions involving excited atoms. *Plasma*, *3*(1), 12–26. <https://doi.org/10.3390/plasma3010003>
- Chen, S., Zeng, R., Zhuang, C., Zhou, X., & Ding, Y. (2016). Experimental study on branch and diffuse type of streamers in leader restrike of long air gap discharge. *Plasma Science and Technology*, *18*(3), 305–310. <https://doi.org/10.1088/1009-0630/18/3/15>
- Cheng, C., Liu, L., He, H., Luo, B., Hu, J., Chen, W., & He, J. (2020). Experimental study of the dynamics of leader initiation with a long dark period. *Journal of Physics D: Applied Physics*, *53*(20), 205203. <https://doi.org/10.1088/1361-6463/ab7625>
- D'alessandro, F., Kossmann, C. J., Gaivoronsky, A. S., & Ovsyannikov, A. G. (2004). Experimental study of lightning rods using long sparks in air. *IEEE Transactions on Dielectrics and Electrical Insulation*, *11*(4), 638–648. <https://doi.org/10.1109/tdei.2004.1324354>

Acknowledgments

The work leading to this paper was supported by a grant from the Hong Kong Polytechnic University. MB would like to acknowledge the financial support of the Swedish strategic research program StandUp for Energy. The authors would like to greatly appreciate LIU Xiaopeng, GAN Quan, GUO Lili, and YE Zhi for their help to carry out the experiments.

- Domens, P., Gibert, A., Dupuy, J., & Hutzler, B. (1991). Propagation of the positive streamer-leader system in a 16.7 m rod-plane gap. *Journal of Physics D: Applied Physics*, 24(10), 1748–1757. <https://doi.org/10.1088/0022-3727/24/10/009>
- Dwyer, J. R., Saleh, Z., Rassoul, H. K., Concha, D., Rahman, M., Cooray, V., et al. (2008). A study of X-ray emission from laboratory sparks in air at atmospheric pressure. *Journal of Geophysical Research*, 113(D23), D23207. <https://doi.org/10.1029/2008jd010315>
- Ebert, U., Nijdam, S., Li, C., Luque, A., Briels, T., & van Veldhuizen, E. (2010). Review of recent results on streamer discharges and discussion of their relevance for sprites and lightning. *Journal of Geophysical Research*, 115(A7). <https://doi.org/10.1029/2009ja014867>
- Gallimberti, I. (1979). The mechanism of the long spark formation. *Journal de Physique. Colloques*, 40(C7), C7-193–C197-250. <https://doi.org/10.1051/jphyscol:19797440>
- Gallimberti, I., Bacchiega, G., Bondiou-Clergerie, A., & Lalande, P. (2002). Fundamental processes in long air gap discharges. *Comptes Rendus Physique*, 3(10), 1335–1359. [https://doi.org/10.1016/s1631-0705\(02\)01414-7](https://doi.org/10.1016/s1631-0705(02)01414-7)
- Gao, Y., Chen, M., Qin, Z., Qiu, Z., Yang, Y., Du, Y. p., et al. (2020). The spatial evolution of upward positive stepped leaders initiated from a 356-m-tall tower in Southern China. *Journal of Geophysical Research: Atmospheres*, 125(2), e2019JD031508. <https://doi.org/10.1029/2019jd031508>
- Goelian, N., Lalande, P., Bondiou-Clergerie, A., Bacchiega, G., Gazzani, A., & Gallimberti, I. (1997). A simplified model for the simulation of positive-spark development in long air gaps. *Journal of Physics D: Applied Physics*, 30(17), 2441–2452. <https://doi.org/10.1088/0022-3727/30/17/010>
- Gu, J., Huang, S., Fu, Y., Chen, W., Cheng, D., Shi, W., et al. (2020). Morphological characteristics of streamer region for long air gap positive discharge. *Journal of Physics D: Applied Physics*, 54(2), 025205. <https://doi.org/10.1088/1361-6463/abb6b3>
- Hare, B. M., Scholten, O., Dwyer, J., Trinh, T. N. G., Buitink, S., Ter Veen, S., et al. (2019). Needle-like structures discovered on positively charged lightning branches. *Nature*, 568(7752), 360–363. <https://doi.org/10.1038/s41586-019-1086-6>
- He, J., Wang, X., Zhao, X., Lee, J., Du, Y., Liu, X., et al. (2022). Schlieren techniques for observations of long positive sparks: Review and application. *High Voltage*, 7(5), 1–15. <https://doi.org/10.1049/hve2.12225>
- Huang, S., Chen, W., Pei, Z., Fu, Z., Wang, L., He, T., et al. (2020). The discharge preceding the intense reillumination in positive leader steps under the slow varying ambient electric field. *Geophysical Research Letters*, 47(3), e2019GL086183. <https://doi.org/10.1029/2019gl086183>
- Jiang, Z. L., He, J. J., Zhao, X. G., Xiao, P., & Yang, Y. C. (2018). Distribution of stems around the HV electrode in a 0.74-m air gap under positive pulses. *IEEE Transactions on Dielectrics and Electrical Insulation*, 25(1), 372–375. <https://doi.org/10.1109/tdei.2018.006935>
- Kochkin, P. O., Nguyen, C. V., van Deursen, A. P., & Ebert, U. (2012). Experimental study of hard X-rays emitted from metre-scale positive discharges in air. *Journal of Physics D: Applied Physics*, 45(42), 425202. <https://doi.org/10.1088/0022-3727/45/42/425202>
- Kochkin, P. O., van Deursen, A. P., & Ebert, U. (2014a). Experimental study of the spatio-temporal development of metre-scale negative discharge in air. *Journal of Physics D: Applied Physics*, 47(14), 145203. <https://doi.org/10.1088/0022-3727/47/14/145203>
- Kochkin, P. O., van Deursen, A. P., & Ebert, U. (2014b). Experimental study on hard X-rays emitted from metre-scale negative discharges in air. *Journal of Physics D: Applied Physics*, 48(2), 025205. <https://doi.org/10.1088/0022-3727/48/2/025205>
- Köhn, C., Chanrion, O., Babich, L. P., & Neubert, T. (2018). Streamer properties and associated x-rays in perturbed air. *Plasma Sources Science and Technology*, 27(1), 015017. <https://doi.org/10.1088/1361-6595/aa5d8>
- Kostinskiy, A. Y., Syssoev, V. S., Bogatov, N. A., Mareev, E. A., Andreev, M. G., Bulatov, M. U., et al. (2018). Abrupt elongation (stepping) of negative and positive leaders culminating in an intense corona streamer burst: Observations in long sparks and implications for lightning. *Journal of Geophysical Research: Atmospheres*, 123(10), 5360–5375. <https://doi.org/10.1029/2017jd027997>
- Les Renardières Group. (1974). Research on long gap discharges at Les Renardières-1973 results. *Electra*, 35, 49–156.
- Les Renardières Group. (1977). Positive discharge in long air gaps at Les Renardières-1975 results and conclusions. *Electra*, 53, 31–153.
- Li, B., Li, X., Fu, M., Zhuo, R., & Wang, D. (2018). Effect of humidity on dielectric breakdown properties of air considering ion kinetics. *Journal of Physics D: Applied Physics*, 51(37), 375201. <https://doi.org/10.1088/1361-6463/aad5b9>
- Li, Y., Li, H., Liu, Z., Fu, Y., Luo, H., Zou, X., & Wang, X. (2021). Breakdown, discharge modes, and gaseous recovery of atmospheric air with repetitive 10 ns pulses. *Physics of Plasmas*, 28(7), 073510. <https://doi.org/10.1063/5.0057340>
- Liu, L., & Becerra, M. (2016). On the transition from stable positive glow corona to streamers. *Journal of Physics D: Applied Physics*, 49(22), 225202. <https://doi.org/10.1088/0022-3727/49/22/225202>
- Liu, L., & Becerra, M. (2017). Gas heating dynamics during leader inception in long air gaps at atmospheric pressure. *Journal of Physics D: Applied Physics*, 50(34), 345202. <https://doi.org/10.1088/1361-6463/aa7c71>
- Liu, L., & Becerra, M. (2018). On the critical charge required for positive leader inception in long air gaps. *Journal of Physics D: Applied Physics*, 51(3), 035202. <https://doi.org/10.1088/1361-6463/aa9fa6>
- Liu, N. (2010). Model of sprite luminous trail caused by increasing streamer current. *Geophysical Research Letters*, 37(4). <https://doi.org/10.1029/2009gl042214>
- Luque, A., & Ebert, U. (2010). Sprites in varying air density: Charge conservation, glowing negative trails and changing velocity. *Geophysical Research Letters*, 37(6). <https://doi.org/10.1029/2009gl041982>
- Luque, A., & Ebert, U. (2014). Growing discharge trees with self-consistent charge transport: The collective dynamics of streamers. *New Journal of Physics*, 16(1), 013039. <https://doi.org/10.1088/1367-2630/16/1/013039>
- Marskar, R. (2019). Adaptive multiscale methods for 3D streamer discharges in air. *Plasma Research Express*, 1(1), 015011. <https://doi.org/10.1088/2516-1067/aafc7b>
- Morrow, R., & Sato, N. (1999). The discharge current induced by the motion of charged particles in time-dependent electric fields; Sato's equation extended. *Journal of Physics D: Applied Physics*, 32(5), L20–L22. <https://doi.org/10.1088/0022-3727/32/5/005>
- Nag, A., Cummins, K. L., Plaisir, M. N., Wilson, J. G., Crawford, D. E., Brown, R. G., et al. (2021). Inferences on upward leader characteristics from measured currents. *Atmospheric Research*, 251, 105420. <https://doi.org/10.1016/j.atmosres.2020.105420>
- Nijdam, S., Teunissen, J., & Ebert, U. (2020). The physics of streamer discharge phenomena. *Plasma Sources Science and Technology*, 29(10), 103001. <https://doi.org/10.1088/1361-6595/abaa05>
- Nijdam, S., Wormeester, G., Van Veldhuizen, E. M., & Ebert, U. (2011). Probing background ionization: Positive streamers with varying pulse repetition rate and with a radioactive admixture. *Journal of Physics D: Applied Physics*, 44(45), 455201. <https://doi.org/10.1088/0022-3727/44/45/455201>
- Niknezhad, M., Chanrion, O., Köhn, C., Holbøll, J., & Neubert, T. (2021). A three-dimensional model of streamer discharges in unsteady airflow. *Plasma Sources Science and Technology*, 30(4), 045012. <https://doi.org/10.1088/1361-6595/abefaf>
- Ono, R. (2018). Rapid temperature increase near the anode and cathode in the afterglow of a pulsed positive streamer discharge. *Journal of Physics D: Applied Physics*, 51(24), 245202. <https://doi.org/10.1088/1361-6463/aac31d>
- Ono, R., & Oda, T. (2003). Formation and structure of primary and secondary streamers in positive pulsed corona discharge—Effect of oxygen concentration and applied voltage. *Journal of Physics D: Applied Physics*, 36(16), 1952–1958. <https://doi.org/10.1088/0022-3727/36/16/306>

- Petrov, N., Avanskii, V., & Bombenkova, N. (1994). Measurement of the electric field in the streamer zone and in the sheath of the channel of a leader discharge. *Journal of Technical Physics*, 39(6), 546–551.
- Pu, Y., & Cummer, S. A. (2019). Needles and lightning leader dynamics imaged with 100–200 MHz broadband VHF interferometry. *Geophysical Research Letters*, 46(22), 13556–13563. <https://doi.org/10.1029/2019gl085635>
- Qie, X., Yuan, S., Zhang, H., Jiang, R., Wu, Z., Liu, M., et al. (2019). Propagation of positive, negative, and recoil leaders in upward lightning flashes. *Earth and Planetary Physics*, 3(2), 102–110. <https://doi.org/10.26464/epp2019014>
- Rahman, M., Cooray, V., Ahmad, N. A., Nyberg, J., Rakov, V. A., & Sharma, S. (2008). X rays from 80-cm long sparks in air. *Geophysical Research Letters*, 35(6), L06805. <https://doi.org/10.1029/2007gl032678>
- Saba, M. M. F., de Paiva, A. R., Concollato, L. C., Warner, T. A., & Schumann, C. (2020). Optical observation of needles in upward lightning flashes. *Scientific Reports*, 10(1), 17460. <https://doi.org/10.1038/s41598-020-74597-6>
- Shah, W. A., He, H., He, J., & Yang, Y. (2018). Continuous and discontinuous streamer leader propagation phenomena under slow front impulse voltages in a 10-meter rod-plane air gap. *Energies*, 11(10), 2636. <https://doi.org/10.3390/en11102636>
- Srivastava, A., Jiang, R., Yuan, S., Qie, X., Wang, D., Zhang, H., et al. (2019). Intermittent propagation of upward positive leader connecting a downward negative leader in a negative cloud-to-ground lightning. *Journal of Geophysical Research: Atmospheres*, 124(24), 13763–13776. <https://doi.org/10.1029/2019jd031148>
- van der Velde, O. A., Montanyà, J., López, J. A., & Cummer, S. A. (2019). Gigantic jet discharges evolve stepwise through the middle atmosphere. *Nature Communications*, 10(1), 4350. <https://doi.org/10.1038/s41467-019-12261-y>
- Visacro, S., Guimaraes, M., & Murta Vale, M. H. (2017). Features of upward positive leaders initiated from towers in natural cloud-to-ground lightning based on simultaneous high-speed videos, measured currents, and electric fields. *Journal of Geophysical Research: Atmospheres*, 122(23), 12786–12800. <https://doi.org/10.1002/2017jd027016>
- Wu, B., Lyu, W., Qi, Q., Ma, Y., Chen, L., Rakov, V. A., et al. (2022). High-speed video observations of needles in a positive cloud-to-ground lightning flash. *Geophysical Research Letters*, 49(2), e2021GL096546. <https://doi.org/10.1029/2021gl096546>
- Wu, C., Xie, S., Qi, F. E. I., Li, B., Wan, J., & He, J. (2013). Effect of corona discharges on the inception of positive upward leader-streamer system. *International Journal of Modern Physics B*, 27(28), 1350165. <https://doi.org/10.1142/s0217979213501658>
- Xiao, P., He, J., Zhao, X., Yang, Y., & shah, W. A. (2019). On the stem diameter under positive impulses in long air gaps. *Physics of Plasmas*, 26(6), 063501. <https://doi.org/10.1063/1.5089684>
- Xie, S., He, J., & Chen, W. (2013). An improved model to determine the inception of positive upward leader–streamer system considering the leader propagation during dark period. *Physics of Plasmas*, 20(4), 042107.
- Xie, Y., He, H., He, J., & Wu, C. (2014). The effect of corona discharge on leader initiation in long air gaps. *IEEE Transactions on Plasma Science*, 42(4), 890–895. <https://doi.org/10.1109/tps.2014.2305446>
- Xie, Y., Yue, Y., Ye, H., Yun, L., Zhong, Y., & Zhao, X. (2018). The development characteristics of the discontinuous leader under the positive switching impulse with low rate of voltage rising. *The European Physical Journal - Applied Physics*, 83(2), 20802. <https://doi.org/10.1051/epjap/2018180103>
- Yang, Y., He, J., Zhao, X., & Xiao, P. (2018). Number of stems around the H.V. electrode in a 0.74-m air gap under positive impulse. *Physics of Plasmas*, 25(10), 103513. <https://doi.org/10.1063/1.5055256>
- Zeng, R., & Chen, S. (2013). The dynamic velocity of long positive streamers observed using a multi-frame ICCD camera in a 57 cm air gap. *Journal of Physics D: Applied Physics*, 46(48), 485201. <https://doi.org/10.1088/0022-3727/46/48/485201>
- Zhao, X., Becerra, M., Yang, Y., & He, J. (2021). Elongation and branching of stem channels produced by positive streamers in long air gaps. *Scientific Reports*, 11(1), 1–11. <https://doi.org/10.1038/s41598-021-83816-7>
- Zhao, X., He, J., Luo, B., Jia, L., Yang, Y., & Xiao, P. (2017). Relaxation process of the discharge channel near the anode in long air gaps under positive impulse voltages. *Journal of Physics D: Applied Physics*, 50(48), 485206. <https://doi.org/10.1088/1361-6463/aa9266>
- Zhao, X., Liu, L., Yue, Y., He, H., Liu, L., & He, J. (2019). On the use of quantitative Schlieren techniques in temperature measurement of leader discharge channels. *Plasma Sources Science and Technology*, 28(7), 075012. <https://doi.org/10.1088/1361-6595/ab1c3e>
- Zhao, X., Liu, X., Yang, Y., Wang, X., Liu, Y., & He, J. (2021). Observations of the channel illuminations during dark periods in long positive sparks. *Geophysical Research Letters*, 48(4), e2020GL091815. <https://doi.org/10.1029/2020gl091815>
- Zhao, X., Wang, X., Liu, X., Liu, Y., Gan, Q., Qi, R., & He, J. (2021). Re-illumination of streamer stems under either rising or non-changing positive electric fields in long air gaps. *AIP Advances*, 11(5), 055303. <https://doi.org/10.1063/5.0050952>